

# Anchoring of *ex-situ* MOF-199 and MOF-UiO-66-NH<sub>2</sub> onto TEMPO-oxidized cotton: potential antibacterials

Sergio Alejandro Torres-Cortés<sup>1\*</sup> , Mauricio Velasquez<sup>2</sup>  and César Sierra<sup>1</sup> 

<sup>1</sup>Grupo de Investigación en Macromoléculas, Departamento de Química, Facultad de Ciencias, Universidad Nacional de Colombia, Bogotá, Colombia

<sup>2</sup>Estado Sólido y Catálisis Ambiental – ESCA, Departamento de Química, Facultad de Ciencias, Universidad Nacional de Colombia, Bogotá, Colombia

\*satorresc@unal.edu.co

## Abstract

This study reports the *ex-situ* anchoring of two metal organic frameworks (MOF-199 and MOF UiO-66-NH<sub>2</sub>) onto TEMPO-oxidized cotton fibers. While *in-situ* anchoring methodologies are reported, *ex-situ* protocols are underreported despite their advantages in industrial scaling-up and control. The functionalized composites were characterized after 48 h of Soxhlet treatment. X-ray diffraction and infrared spectra confirmed MOFs anchorage through super positioning signals corresponding to cotton and MOFs. Likewise, X-ray photoelectron spectra (XPS) show the presence of Cu<sup>2+</sup> (4.73% molar ratio) and Zr<sup>4+</sup> (12.06%) coordinated to the -COO groups of the organic linkers, indicating a stable chemical interaction. Finally, SEM confirmed the expected MOF morphology. The potential antibacterial activity of these materials was evaluated. The assays revealed a bacteriostatic effect for MOF UiO-66-NH<sub>2</sub>@cotton, even after 48 h of contact. Meanwhile, the MOF-199@cotton showed a bactericide effect under the same conditions.

**Keywords:** antibacterial material, *ex-situ* chemical anchorage, MOF, TEMPO-oxidation.

**How to cite:** Torres-Cortés, S. A., Velasquez, M., & Sierra, C. (2025). Anchoring of *ex-situ* MOF-199 and MOF-UiO-66-NH<sub>2</sub> onto TEMPO-oxidized cotton: potential antibacterials. *Polímeros: Ciência e Tecnologia*, 35(1), e20250007. <https://doi.org/10.1590/0104-1428.20240068>

## 1. Introduction

The chemical modification of textile fibers is a broad field that continues to be explored due to the importance of its applications. It is highly spread for industrial use in food, textiles, pharmaceuticals, and environmental remediation<sup>[1]</sup>. Cotton, the principal product obtained from natural cellulose, is a desired material principally for its abundance of -OH groups, which make it an ideal material for surface modifications that include oxidation, carboxylation, and carboxymethylation, among others<sup>[2,3]</sup>.

Various inorganic and metalorganic-like materials have been evaluated to carry out modifications on the surface of cotton<sup>[4-6]</sup>. However, the use of metal-organic frameworks (MOFs) to functionalize fibers is a promising and innovative strategy that could offer significant advantages over traditional methods. The unique physicochemical properties of MOFs, such as their porosity, surface area, and structural flexibility, make them exceptional materials for a wide range of applications<sup>[7-9]</sup>. In fact, antibacterial properties of nanomaterials like MOFs depend on the chemical properties given to these materials and the synergy between metal centers and ligands. MOFs can act as metal reservoirs, allowing their gradual release, a mechanism to which their antibacterial activity is attributed. Once released, the metallic species undergo biocidal activity by

internalization and damage in DNA and protein synthesis or by inhibiting membrane synthesis<sup>[10,11]</sup>.

Nevertheless, direct applications of MOFs at the industrial level have some issues associated with the thermal and mechanical fragility and powder-like aggregation state, which can lead to the leaching of the metal cluster or the destruction of the initial structure. One way to solve this problem is by anchoring MOFs to textile fibers through chemical bonds between the metallic coordination nodes of MOFs and functional groups present on the fiber surface. Then, in most cases, textile fibers need to be functionalized before the anchorage to produce the coordination sites required to attach MOFs<sup>[12]</sup> is a methodology in which a sodium bromo- or chloroacetate solution, in the presence of a base, is used to convert primary and secondary -OH cellulose groups into carboxymethyl-ether groups. On the other hand, TEMPO (2,2,6,6-tetramethylpiperidinyloxy) carboxylation is a regioselective, catalytic, and easy-to-do reaction in which this stable free radical is used in the presence of NaClO as primary oxidant, NaClO<sub>2</sub> as co-oxidant and NaBr as reducing agent to oxidate primary -OH groups into carboxylate groups. This methodology, first reported by de Nooy et al.<sup>[13]</sup>, has been widely spread to oxidate fique, starch, and pullulan, among other cellulosic materials<sup>[14,15]</sup>. Biermann published the first attempt to introduce an MOF

into a cellulosic material<sup>[16]</sup>. Like this, other works have been reported with the goal to anchor the MOF structures on fibers<sup>[17-19]</sup>. Some of them are related to the antibacterial applications. However, all these works are focused on the in-situ anchored procedures where most of the synthesized MOF is not attached efficiently to the modified fiber, showing low MOF charges. Additionally, functionalized materials commonly present a substantial leaching of the MOF. Because of these problems, few authors have reported ex-situ approaches to anchor previously synthesized MOFs on modified textile fibers. These methodologies can offer several advantages, such as higher amounts of anchored material, stronger interactions between MOF and fiber, and the possibility of higher recovery of non-anchored the MOF material<sup>[20-22]</sup>. Therefore, in the present work, the chemical anchoring of *ex-situ* obtained MOF-199 and MOF UiO-66-NH<sub>2</sub> onto TEMPO/NaClO/NaClO<sub>2</sub> oxidized cotton fibers is reported, and finally, their antibacterial potential was tested against *E. coli* and *S. aureus*.

## 2. Materials and Methods

### 2.1 Materials

Free radical 2,2,6,6-tetramethyl-1-piperidinil-oxyl (TEMPO) was obtained from Sigma-Aldrich Chemie® GmbH. 15% sodium hypochlorite was purchased from Químicos J.J. Ltda. Reference textile cotton 100% (TIC 400, 98 g m<sup>-2</sup>, 1 m<sup>2</sup>) was obtained from Testfabrics Inc. Zirconium chloride, sodium chloride, acetone, ethanol (EtOH), and copper (II) nitrate trihydrate (Cu(NO<sub>3</sub>)<sub>2</sub> · 3H<sub>2</sub>O) were obtained from Merck KgaA. 2-Amino terephthalic acid (H<sub>2</sub>BDCNH<sub>2</sub>), methanol, and deionized water were purchased from Merck Millipore®. 1,3,5-Benzene tricarboxylic acid (H<sub>3</sub>BTC), zinc nitrate hexahydrate, *N,N,N*-triethylamine, TEA, and dimethylformamide (DMF) were obtained from PanReac AppliChem®. The reactants were used as purchased without purification.

### 2.2 MOFs synthesis

With these materials the procedures of MOF synthesis (Scheme S1a and S1b), cotton functionalization (Scheme S2), and *ex-situ* chemical MOF anchoring (Scheme S3) were carried out similar to our previous report<sup>[23]</sup>.

### 2.3 Materials characterization

The MOFs and the fibers were characterized separately. Then, the fibers functionalized with the MOFs were characterized after 48 h of Soxhlet treatment using a methanol-water solution. Thus, the structure and chemical composition of all materials were analyzed by Attenuated Total Reflectance-Fourier Transformed Infrared spectroscopy (FTIR-ATR). The spectra were recorded with a Shimadzu® FTIR solutions spectrophotometer with an ATR module (attenuated total reflectance) with germanium crystal (4000-600 cm<sup>-1</sup>). The X-ray diffraction (XRD) patterns were recorded using a Philips Analytical® PW3050/60 diffractometer with Cu anode (K $\alpha$ : 1.54056 Å), operated at 45 kV voltage and 40 mA acceleration current. The X-ray photoelectron (XPS) spectra were measured with an X-ray photoelectronic spectrometer X (NAP-XPS) Specs® with a PHOIBOS 150 1D-DLD analyzer,

using an Al-K $\alpha$  monochromatic (1486.7 eV, 13 kV, 100 W) source with a passing energy of 90 eV. High-resolution spectra were recorded using an analysis area of 300  $\mu$ m x 700  $\mu$ m and a 20eV pass. Data were acquired with 0.5 eV steps. All the binding energies were calibrated with the C<sub>1s</sub> binding energy fixed at 284.6 eV as an internal reference. SEM micrographs were recorded using a Jeol-JSM-6490 probe for EDX analysis, operated at an acceleration 20 kV beam voltage, and using a Jeol-JSM-6490 probe with a 20 kV beam and a magnification power of 3000x. The quantification of the carboxylate groups after the fiber oxidation were determined by a coulometric titration. The carboxylated fiber was introduced in a glass reactor and pretreated with HCl 0.1 M solution to protonate the carboxylate groups. Then, the fiber was washed to obtain the conductivity of the water. The titration was carried out using 20 mL of 0.1 M KCl as the electrolyte, a Pt electrode (cathode), an Ag electrode (anode), and the pH sensor as the indicator electrode in the acid-base titration. The electrodes were connected in series through a multimeter, and a constant current of 9.97 mA was applied. Finally, UV-visible analyses of bacterial cultures were performed using a Thermo Evolution-3000 with a double beam and xenon lamp.

## 3. Results and Discussions

### 3.1 Characterization of MOF-199 and UiO-66-NH<sub>2</sub>

For the synthesized MOF-199, the FTIR-ATR signals and their corresponding vibration modes were found at 1644 cm<sup>-1</sup> (-C=O, stretching); 1450 cm<sup>-1</sup> (O-C=O, bending); 1372 cm<sup>-1</sup> (v<sub>as</sub> =C-O, stretching); 1112 cm<sup>-1</sup> (O-C=O, stretching) and 725 cm<sup>-1</sup> (Cu-O, stretching) (Figure S1a). These signals agree with the previously reported analysis<sup>[24]</sup>. The band over 3300 cm<sup>-1</sup> corresponds to the presence of remanent water. Likewise, The XRD pattern (Figure S1b) shows the characteristic peaks at ( $^{\circ}$  2 $\theta$ ) = 5.75 (200); 9.57 (220); 11.68 (222); 13.56 (400); 15.12 (420); 17.56 (422) which confirm the formation of the material.

On the other hand, for the MOF UiO-66-NH<sub>2</sub>, the FTIR-ATR signals (Figure S2a) and its corresponding vibration modes were found at 3868 cm<sup>-1</sup> (N-H, stretching); 1652 cm<sup>-1</sup> (-C=O, stretching), 1567 cm<sup>-1</sup> (O-C=O, bending); 1388 cm<sup>-1</sup> (N-H, bending) and 764 cm<sup>-1</sup> (p C-C, stretching) which are the typical bands of this MOF as were previously reported<sup>[25]</sup>. Over 3800 cm<sup>-1</sup> are appreciated the bands of symmetric and asymmetric stretching of N-H bonds in 2-amino terephthalic acid.

The XRD patterns in Figure S2b show the 2 $\theta$  peaks at 7.60° (111); 8.92° (002); 12.34° (004); 22.44° (115), and 25.95° (006), which match well with the reported standard pattern<sup>[26]</sup>.

### 3.2 characterization of cotton fibers

The pure and carboxylated cotton fibers were also characterized by FTIR-ATR and XRD spectroscopies. The infrared spectrum of the pure cotton (Figure 1a) shows typical signals at 3346 cm<sup>-1</sup> (stretching, O-H), 1315 (flexion, C-H in cellulose skeleton), 1160-1107 cm<sup>-1</sup> (stretching, C-O alcohol), and 1050 cm<sup>-1</sup> (stretching, C-O primary alcohol), which indicate the presence of the hydroxyl groups. Consequently, the XRD pattern (Figure 1b) shows the typical

peaks of the cotton structure ( $2\theta$ ) = 14.88, 16.51, 22.87 and 34.26. According to previous reports, the crystalline domains in cotton textiles are less reactive and more inert than the amorphous ones. Nevertheless, the surface modifications onto cotton fibers can diminish the crystalline domains and increase the presence of amorphous domains in cotton fibers<sup>[15]</sup>.

The carboxylated cotton, depicted in Figure 1a, shows an evident transformation with the peak at 1610 cm<sup>-1</sup> corresponding to the presence of -C=O bonds of carboxylate groups, which do not appear in the spectrum of pure cotton. Although the complementary band at 3346 cm<sup>-1</sup> does not show a relevant change, the loss of symmetry in this for the carboxylated fiber can be interpreted as the loss of -OH groups from primary alcohols that became carboxylate groups after the treatment. Likewise, The XRD spectra in Figure 1b show no appreciable modification of the crystalline properties of the textile, and the diffraction peaks are in good agreement with a previous report<sup>[27]</sup>.

From the FTIR-ATR results, the carbonyl index (IC) was calculated, which provides an estimation of the functionalization of the cellulose. According to eq. 1,  $A_{CO}$  is the absorbance of the carbonyl stretching band (1610 cm<sup>-1</sup>), and  $A_{RB}$  is the absorbance of the reference band, which should be a peak with constant intensity in both pure and carboxylated cotton spectra. In this work, the band at 1315 cm<sup>-1</sup> was chosen, as suggested in a former report<sup>[28]</sup>. On the other hand, the crystallinity index (CI, eq. 2). This was estimated using the empirical method of Segal et al.<sup>[29]</sup> through the relation of intensities of the diffraction peaks at 22.5°  $2\theta$ , corresponding to (200) peak ( $I_{22.5}$ ), and the intensity of the amorphous fraction ( $I_{AM}$ ), corresponding to 18°  $2\theta$ . The carbonyl and crystallinity indexes were measured for the cotton textile before and after modification, and the results are summarized in Table 1.

$$IC(\%) = \frac{A_{CO}}{A_{RB}} \times 100 \quad (1)$$

$$CI(\%) = \frac{I_{22.5} - I_{am}}{I_{22.5}} \times 100 \quad (2)$$

The CI results show a lower value for the carboxylated fiber, which may be explained by the fact that some crystalline

domains suffer a loss of crystallinity with the chemical treatment. According to earlier reports regarding the characterization of cellulose, the crystallinity index decreases significantly with extensive large reaction times. In this study, the reaction time did not exceed 2 hours, and according to the XRD spectra in Figure 1b, the crystal domain was not changed. On the other hand, the result of the carbonyl index for the TEMPO-oxidized cotton fibers shows a higher percentage of carbonyl groups on their surface, giving evidence of the effectiveness of the functionalization.

As previously described, the concentration of carboxylic groups (-COOH) was tested by coulometric titration, confirming FTIR-ATR observations. The titration curves were analyzed by using the OriginPro® software, and the number of carboxylic groups was calculated using eq. 3, where  $t_{END\ POINT}$  corresponds to the time (expressed in seconds) in which the titration reaches the endpoint,  $i$  is the constant current (in Amperes) provided by the potentiostat. The results are depicted in Table 2 (titration experiments were carried out several times, the values herein reported are representative amounts, selected as the best and most reliable data).

$$\frac{mmol\ COOH}{g\ textile} = t_{end\ point} (s) \cdot i (A) \cdot \frac{1\ mol\ e^-}{96485,33\ C} \cdot \frac{1\ mol\ H^+}{1\ mol\ e^-} \quad (3)$$

$$\frac{1\ mol\ COOH}{1\ mol\ H^+} \cdot \frac{1000\ mmol}{1\ mol} \cdot \frac{1}{g\ textile}$$

These results from two different experiments show good repeatability of the functionalization method, where an amount of around 0.066 mmol/g was obtained. These results are in good agreement, or even better, with the previous

**Table 1.** Obtained results of CI and IC for cotton composites.

Fiber	Carbonyl index (CI)	Crystallinity index (IC)
	(%)	(%)
Cotton	-	68.76
Cotton-COOH	71.43	49.83

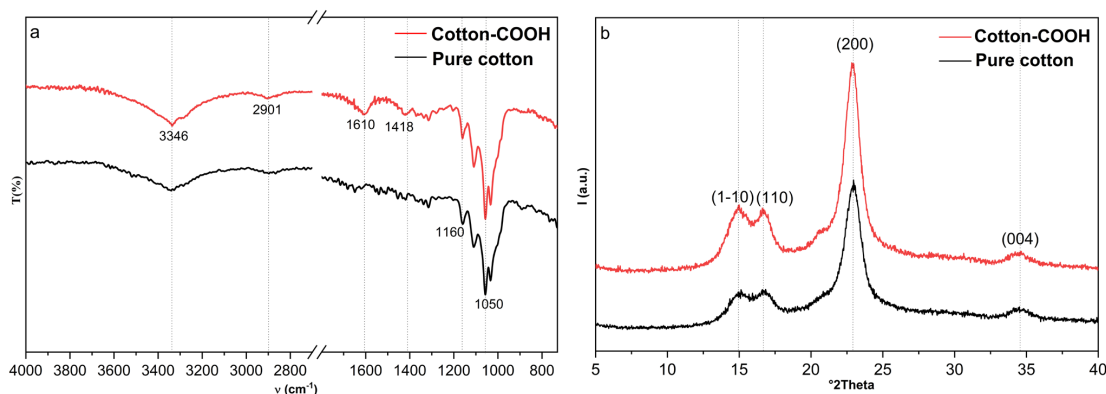


**Figure 1.** (a) FTIR-ATR spectrum of pure cotton (black) and cotton-COOH (red) and (b) DRX pattern of pure cotton (black) and cotton-COOH (red).

reports of COOH concentrations onto cellulosic fibers also used for anchoring *in-situ* obtained metal nanoparticles<sup>[30]</sup>.

In previous work, similar functionalization was made for polyester/cotton (PETco) fibers for the same applications. As expected, the presence of the synthetic material mixed with cotton halves the performance of fiber functionalization. Therefore, the performance of these pure cotton fibers in biological applications is expected to be higher<sup>[31,32]</sup>.

### 3.3 Chemical immobilization of *ex-situ* MOF-199@ cotton

Figure 2a shows the FTIR-ATR spectra of MOF-199, carboxylated cotton (Cotton-COOH), and the MOF anchored onto carboxylated cotton (MOF-199@cotton). In general, for the MOF-199@cotton spectrum, the same signals of MOF-199 (specifically at 725, 1372, 1546, and 1644  $\text{cm}^{-1}$  can be observed). Likewise, in this case, the signals of carboxylated cotton, specifically at 1056 and 1610  $\text{cm}^{-1}$ , which overlap with the signal at 1644  $\text{cm}^{-1}$ . However, the disappearance of the signal at 3328  $\text{cm}^{-1}$  characteristics of carboxylic groups indicates a change in this vibration mode due to the formation of new chemical bonds between MOF-199 and carboxylic groups in the cotton. Additionally, after the anchorage process, the remanent signal around 1056  $\text{cm}^{-1}$  reveals the presence of non-functionalized hydroxyl groups, which implies that this process can be improved.

On the other hand, the XRD pattern of the hybrid MOF/textile material (Figure 2b) can be analyzed as a superposition of the diffraction pattern of MOF-199 and the textile at low diffraction angles, where the MOF peaks are not overlapped by the broad and high peak at  $22.5^\circ 2\theta$ , corresponding to the crystalline phase of cotton, which is in good agreement with previous

reports. These results complement and support the analyses made by infrared confirming the anchorage of the MOF-199 onto the carboxylated fiber.

The obtained materials also underwent SEM analysis to verify the morphology of the crystals of MOF after the chemical immobilization. The SEM micrographs in Figure 3a and 3b show irregular particles covering the fibers. However, some crystals of MOF-199 maintained the octahedral morphology after the anchorage. The crystals have a broad size distribution, from 1 to 40  $\mu\text{m}$ . This can be attributed to the prolonged times of stirring in suspension, which could affect the form and size of the crystals. The complementary EDX results also confirms the presence of copper (Figure S3).

The MOF-199@cotton composites were also analyzed by XPS. The general XPS spectrum of this material is shown in Figure S5a. This spectrum shows the characteristic signals for Cu2p, Zn2p, O1s and C1s, confirming the presence of Cu and Zn species in chemical interactions with cotton-COOH textile fibers near the surface. The binding energy corresponding to Zn2p is observed at 1044.4 and 1021.3 eV (Figure S5c), indicating that the cation exchange with the copper was incomplete. The deconvoluted signals in the high-resolution spectrum of C1s in Figure S5b show the different chemical interactions of the carbon in the organic linkers at 284.6 and 287.9 eV and the carbon related to the bond with the oxygen and metal core at 286.1 eV. Likewise, the signals observed in the O1s (536-526 eV) and Cu2p (940-930 eV) high-resolution spectra are shown in Figure 4a and 4b, respectively. The analysis of these spectra was reported in the previous work for *ex-situ* anchored MOFs in PET-cotton fabrics<sup>[23]</sup>. The most characteristic interactions found from the XPS spectrum of MOF-199@cotton are summarized in Table 3. Therefore, these chemical interactions confirm the presence of the MOF-199 on the surface of the textile fibers. XPS analyses of MOF-199@cotton fibers also helped to estimate the concentration of  $\text{Cu}^{2+}$  and  $\text{Zn}^{2+}$  on the surface. As shown in Table 3, the surface concentration of  $\text{Cu}^{2+}$  was quantified as 4.47% atomic, whereas, for  $\text{Zn}^{2+}$ , the concentration was 2.52%. This critical amount of remanent  $\text{Zn}^{2+}$  suggests that the yield of the cation exchange process was lower. Therefore, optimizing the synthesis parameters may improve the amount of copper in the MOF.

**Table 2.** Concentration of surface COOH groups in cotton-COOH fiber.

Experiment	Mass of carboxylated cotton fiber (g)	[COOH] (mmol/g)
1	285.23	0.064
2	295.84	0.068

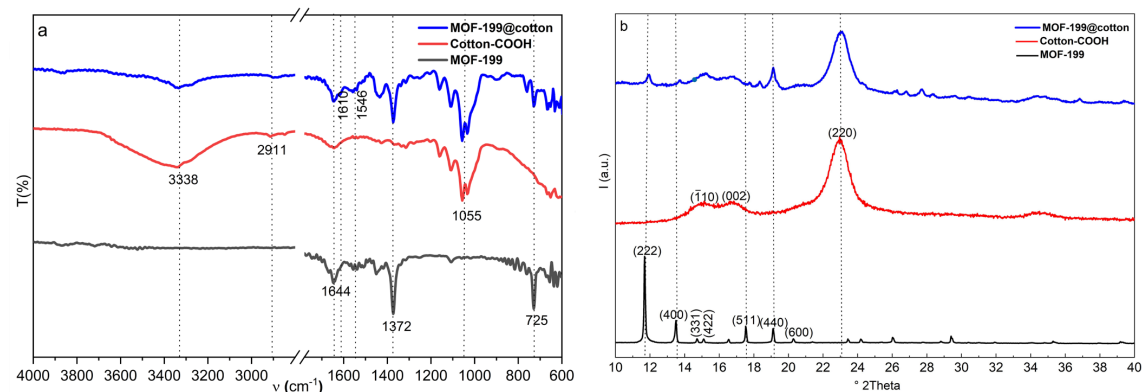


**Figure 2.** a) FTIR-ATR spectra of cotton-COOH (red), MOF-199 (black), and MOF-199@cotton (blue). b) XRD spectra of cotton-COOH (red), MOF-199 (black), and MOF-199@cotton (blue).

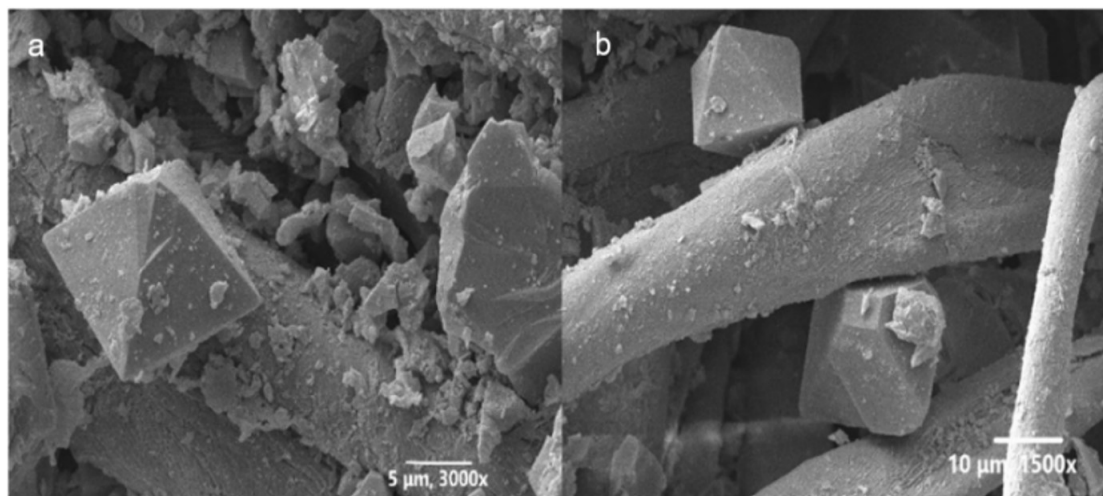


Figure 3. SEM images at (a) 5  $\mu\text{m}$  - 3000x and (b) 10  $\mu\text{m}$  - 1500x for MOF-199@cotton material.

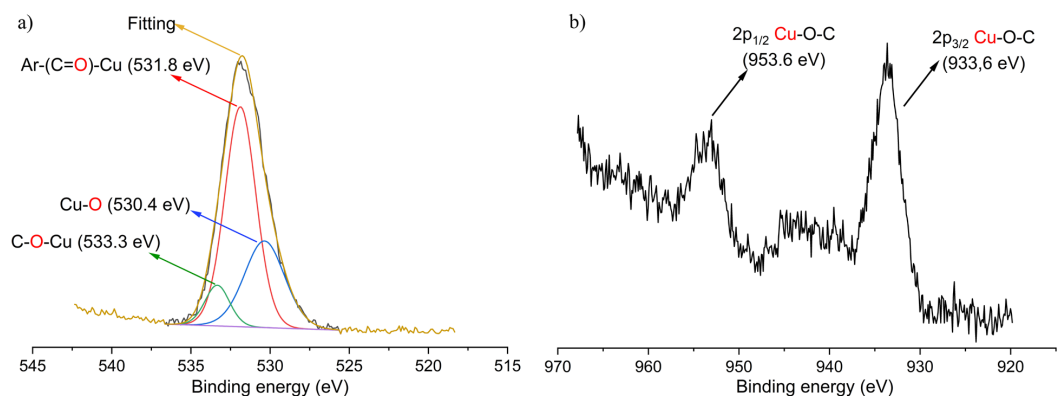


Figure 4. Deconvoluted XPS signals for a) O1s and b) Cu2p for MOF-199@cotton materials.

Table 3. Significant XPS atomic interactions in MOF-199@cotton materials.

Species	Atomic %	Interaction	B.E. (eV)
C(1s)	41.29	C-Ar; Ar-C-O-Cu	284.6; 287.9
O(1s)	51.45	Ar-(C=O)-OH; C-O-Cu	531.8; 533.3
Cu(2p)	4.73	Cu2p(3/2)-O-C; Cu2p(1/2)-O-C	953.6; 933.6
Zn(2p)	2.52	Zn2p(3/2)-O-C; Zn2p(1/2)-O-C	1044.4; 1021.3

### 3.4 Chemical immobilization of ex-situ MOF-UiO-66-NH<sub>2</sub>@cotton

Regarding MOF UiO-66-NH<sub>2</sub>@cotton, the chemical immobilization of MOF UiO-66-NH<sub>2</sub> was made according to the same procedure depicted in Scheme S3. In the case of this MOF, there was no previous treatment of the carboxylated fibers with Zn<sup>2+</sup> solution to make a cationic exchange with metal ions in the MOF structure, as previously explained for MOF-199. The main reason is the strong chemical interaction between the Zr<sup>4+</sup> and carboxylate ligands in textile fibers due to Pearson's hard acid character of Zr<sup>4+</sup> and the

nucleophilic nature of the carboxylates. Specifically, Zr<sup>4+</sup> is a little charge-concentrated cation with low polarizability and a highly energetic LUMO orbital without readily excitable electrons<sup>[32]</sup>. The FTIR-ATR spectrum of MOF UiO-66-NH<sub>2</sub>@cotton in Figure 5a shows the expected signals as an overlapping of MOF UiO-66-NH<sub>2</sub> and carboxylated textile fiber bands. The most relevant signals observed are the band's disappearance at 3868 cm<sup>-1</sup> in the composite spectrum, corresponding to the disappearance of -OH from carboxy groups by coordination with the Zr<sup>4+</sup> cation. Additionally, the intensity of the signal at 1652 cm<sup>-1</sup> increased by the overlapping of the O=C=O of the carboxylate groups in

cotton and in BDC ligands. Finally, at  $764\text{ cm}^{-1}$ , the band appears to be related to Zr-O stretching mode in MOF UiO-66-NH<sub>2</sub><sup>[33]</sup>.

The XRD spectra of the composites, shown in Figure 5b, describe a good overlapping of the signals of the diffraction peaks of MOFs over the textile fibers. As mentioned before, the oxidation treatments with TEMPO, in the case of these experiments, exert no influence on the diffraction pattern of the fibers. As seen in the XRD diffraction pattern for pure cotton in Figure 1b (black) and for cotton-COOH in Figure 1b (red), the peaks corresponding to (110), (110), (200), and (004) diffraction planes for cotton remain with no modifications, maintaining the pristine topology of the hybrid textile/MOF material<sup>[20]</sup>.

The obtained SEM/EDX of MOF UiO-66-NH<sub>2</sub>@cotton composites are shown in Figure 6a and 6b. The micrographs show a semispherical particles of approximately 500 nm to 1  $\mu\text{m}$  which is characteristic of this MOF according with a previous report<sup>[34,35]</sup>. The covering seems to be homogeneous as the size distribution of the MOF particles. Additionally, the EDX spectrum confirms the presence of Zr<sup>4+</sup> cation (Figure S7).

A complementary superficial analysis of the composite was made by XPS. The general spectrum can be seen in Figure S6a, where the binding energy signals corresponding to Zr3d, C1s, O1s, N1s were observed. In the high-resolution spectra of Zr3d (Figure 7b), the presence of Zr<sup>4+</sup> bonded to oxygen is indicated by two signals at 182.8 eV (Zr3d<sub>(5/2)</sub>) and 185.2 eV (Zr3d<sub>(3/2)</sub>), suggesting that the Zr<sup>4+</sup> ion is coordinated to the -COO groups of the organic linkers, but also to the -COO groups of the cotton-COOH. This finding aligns with previous reports by the mentioned authors and by Wagner et al.<sup>[36]</sup>. On the other hand, the deconvoluted O1s spectrum (Figure 7a) in the fiber revealed signals assigned as C-O-Zr (533.2 eV), -C-(C=O)-OH (531.6 eV), and Zr-O (529 eV) based on the research conducted by Ardila-Suárez et al.<sup>[37]</sup>, who investigated the XPS study of three Zr MOFs using H<sub>2</sub>BDC-NH<sub>2</sub> as a linker. The signals containing Zr are particularly significant as a comparison between the general XPS spectrum of carboxylated cotton fibers as a reference (Figure S4) and those of MOF UiO-66-NH<sub>2</sub>@cotton (Figure S6) confirms the occurrence of Zr<sup>4+</sup> ion anchoring. The binding energy of the C-O-Zr and Zr-O bonds remains consistent in the MOF UiO-66-NH<sub>2</sub>@cotton fiber, indicating similar energy as observed

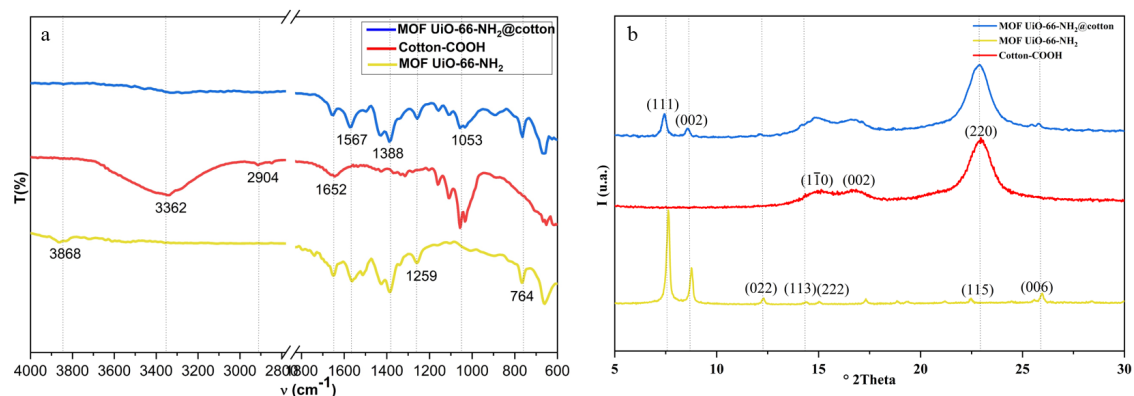


**Figure 5.** (a) FTIR-ATR spectra of cotton-COOH (red), MOF UiO-66-NH<sub>2</sub> (yellow), and cotton@MOF UiO-66-NH<sub>2</sub> (blue). (b) XRD spectra of cotton-COOH (red), MOF UiO-66-NH<sub>2</sub> (yellow), and MOF UiO-66-NH<sub>2</sub>@cotton (blue).

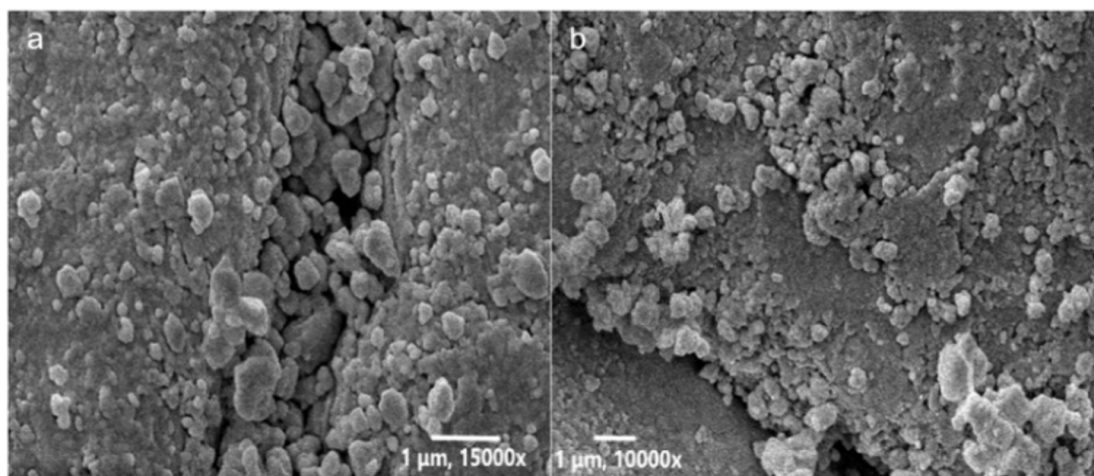


**Figure 6.** SEM images at (a) 15000x and (b) 10000x of MOF UiO-66-NH<sub>2</sub>@cotton.

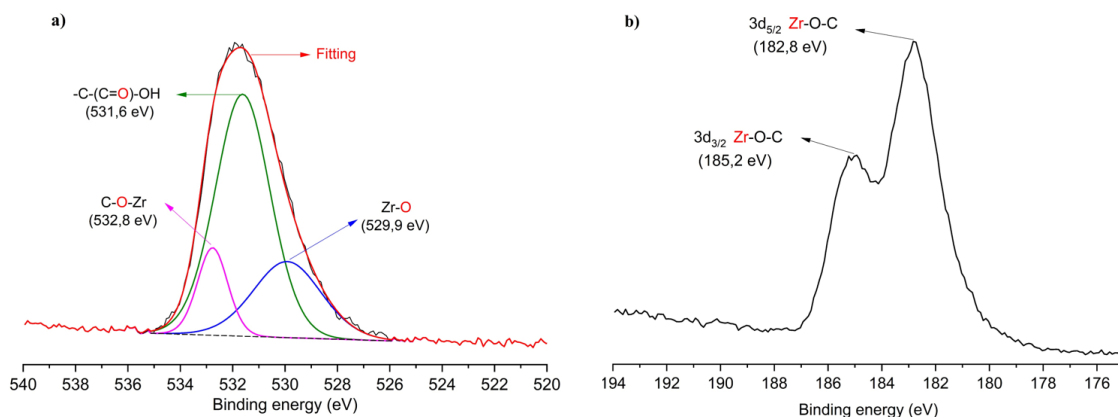


**Figure 7.** High-resolution XPS spectra for (a) O1s and (b) Zr3d in MOF UiO-66-NH<sub>2</sub>@cotton.

**Table 4.** Significant XPS atomic interactions in MOF UiO-66-NH<sub>2</sub>@cotton materials.

Species	Atomic %	Interaction	B.E. (eV)
C(1s)	44.28	C-Ar; Ar-C-O-Zr	284.6; 286.0
O(1s)	41.99	Ar-(C=O)-OH; C-O-Zr	531.6; 532.8
Zr(3d)	12.06	Zr3d(3/2)-O-C; Zr3d(5/2)-O-C	185.2; 182.8
N(1s)	1.67	C-N1s-H	399.3

in the pure state of the MOFs.<sup>[37]</sup> The deconvoluted signals of the other analyzed elements (C1s and N1s) are also present and displayed in Figure S6b and S6c. Finally, Table 4 shows the semiquantitative analysis of these elements. The atomic percentage of Zr<sup>4+</sup> was 12.06, higher than values reported in other studies involving MOFs from the UiO family on this type of fiber<sup>[38]</sup>.

## 4. Inhibition assays

### 4.1 Inhibition assays in solid cultures

The bactericidal experiments conducted with MOFs/cotton systems revealed the formation of inhibitory zones around the fibers in the nutrient agar culture. Compared with preliminary trials using *in-situ* attached MOFs/cotton systems, these results do not show any leaching of MOF, indicating a stronger chemical interaction between the metal-organic framework and the textile fiber. Among the tested systems, MOF-199@cotton and MOF UiO-66-NH<sub>2</sub>@cotton exhibited noticeable inhibitory zones in the *E. coli* assay (Figure S8a). In this case, the MOFs inhibited growth in the contact area with the nutrient gel. However, partial inhibition zones farther from the textile fiber were also observed, in which bacterial growth was present but at a lower rate. The size of halos for the MOF UiO-66-NH<sub>2</sub>@cotton was a little larger than halos formed around MOF-199@cotton ( $\phi$  of 11.3 mm for MOF UiO-66-NH<sub>2</sub>@cotton and 10.7 mm for MOF-199@cotton), the higher metal content in the MOF UiO-66-NH<sub>2</sub>@cotton could explain this. However, under the same observation, it is possible to suggest that MOF-199@cotton has a higher bactericidal potential due to the low metal content.

In the *S. aureus* test (Figure S8b), the MOF-199@cotton also showed a total inhibition in the surroundings of the

textile fibers, and the inhibition halos were larger than those for the MOF UiO-66-NH<sub>2</sub>@cotton in which was observed principally a bacteriostatic effect ( $\phi$  of 7.0 mm for MOF UiO-66-NH<sub>2</sub>@cotton and 16.4 mm for MOF-199@cotton). Surprisingly, the positive control (pure cotton soaked in DMSO) did not inhibit the growth of *E. coli* and *S. aureus*, contradicting previous reports<sup>[39]</sup>. Therefore, assuming that the growth rate of bacteria is directly correlated to the intensity of the color of the coating formed by the culture around the fabric (considering cotton blanks and positive controls), it is possible to conclude that MOF UiO-66-NH<sub>2</sub>@cotton exhibited a mayor bacteriostatic effect. At the same time, MOF-199@cotton displayed a major antibacterial effect.

### 4.2 Inhibition assays in liquid cultures

Considering the outcomes observed in the Petri dish experiments, conducting an analysis using liquid cultures would help validate the previous findings and enable more precise quantification of the antibacterial or bacteriostatic effects of the textiles. The inhibition curves for *E. coli* (Figure S9a) demonstrate a significant inhibitory effect exerted by the textile/MOF systems. Starting with an initial bacterial inoculum of approximately  $2.02 \times 10^8$  (with an  $OD_{625}$  of 0.161), the cotton blank exhibited no inhibition over the 48h duration of the experiment but rather a rapid increase in bacterial growth after 10 h. Conversely, the MOF-199@cotton and MOF UiO-66-NH<sub>2</sub>@cotton systems significantly reduce bacterial populations throughout the experiment. Although the textile/MOF systems resulted in a substantial decrease in the growth rate of *E. coli* compared to the cotton blank (reducing the number of bacteria by at least threefold), complete inhibition or eradication of the bacteria did not occur. Therefore, for these bacteria, it is possible to suggest that these MOFs have mainly a bacteriostatic effect, and

the MOF-199@ cotton also has a bactericide effect. Still, the kinetic of the process is slow. This finding suggests that the copper content in the textile may not directly correlate with antibacterial activity. Similarly, MOFs containing  $Zr^{4+}$ , such as those in the UiO MOF family, have been reported to possess inferior antibacterial properties when obtained *in-situ* compared to MOF-199. The Zr-MOF-based materials are commonly post-functionalized with other biocidal agents like Ag nanoparticles (AgNP) or subjected to ultraviolet light irradiation<sup>[40-42]</sup>. Nevertheless, other factors, such as the strength of the bond between textile fibers and MOF and the size of the MOF crystals, cannot be discounted as potential influences on the intensity of antibacterial activity, as these factors are currently under investigation. For the inhibition against *S. aureus* (Figure S9b), the textile/MOF systems exhibited a significantly more potent inhibition with the MOF-199@ cotton material, reducing the bacterial population by nearly half within 48 hours and confirming the powerful inhibitory effect of copper. In contrast, the inhibitory power of the MOF UiO-66-NH<sub>2</sub>@ cotton with these bacteria was notably weaker within the timeframe of the experiment. Furthermore, comparing the bacterial count at 0 hours with that at 48 hours, it did not reach or fall below the initial count, leading to the conclusion that MOF UiO-66-NH<sub>2</sub>@ cotton textile does not completely inhibit bacterial growth but instead slows it down while maintaining effective population control. It is important to note that during the first 3 hours, population growth is observed for both materials. After this time, the bactericide effect of copper is remarkable, indicating that the growth kinetics of these bacteria is greater than the death kinetics during the first hours.

Finally, Figure S10a and S10b demonstrate that the inhibition was more pronounced and significant for *S. aureus* than *E. Coli*. Figure S6 indicates that the percentage of inhibition was notably higher with the MOF-199@ cotton material (29.91% for *E. coli* and 54.92% for *S. aureus*) compared to the MOF UiO-66-NH<sub>2</sub>@ PETco material after 48 h. It is also worth noting that the contrast of the color (white) in the Petri dish cultures corresponds to the bacterial concentration, and the liquid culture assays support these analyses, as can be observed in Figure S7.

## 5. Conclusions

This article reports a successfully modification of cotton textile fibers via the TEMPO selective oxidation method, resulting in surface functionalization with carboxylate groups capable of anchoring MOFs. This modification enabled the *ex situ* synthesis of MOF-199@ cotton and MOF UiO-66-NH<sub>2</sub>@ cotton composites. These composites demonstrated excellent resistance to Soxhlet washing, indicating that strong chemical interactions formed between the MOFs and the carboxylated cotton fibers. XPS, XRD, and FTIR-ATR analyses confirmed the integration of functional, atomic, and crystalline properties of both cotton and MOF, as well as the coordination between MOF metal centers and the textile fibers. The MOF-199@ cotton composite exhibited a 4.73% Cu<sup>2+</sup> composition in surface, and a notable antibacterial activity against *E. coli* and *S. aureus*, while MOF UiO-66-NH<sub>2</sub>@ cotton showed a composition of 12.06% of Zr<sup>4+</sup> in surface, alongside a bacteriostatic effect with

a trend of increasing efficacy over time. These results highlight the potential of the *ex situ* methodology for developing durable functional textiles with promising antimicrobial properties. The approach allowed for precise MOF anchoring, leading to stable and well-integrated composite materials suitable for various applications, particularly in textiles with enhanced performance.

## 6. Author's Contribution

- **Conceptualization** – Sergio Torres-Cortés; César Sierra
- **Data curation** – Sergio Torres-Cortés; Mauricio Velasquez
- **Formal analysis** – Sergio Torres-Cortés; Mauricio Velasquez
- **Funding acquisition** – Sergio Torres-Cortés; César Sierra
- **Investigation** – Sergio Torres-Cortés; Mauricio Velasquez
- **Methodology** – Sergio Torres-Cortés; Mauricio Velasquez
- **Project administration** – César Sierra
- **Resources** – Mauricio Velasquez; César Sierra
- **Software** – NA
- **Supervision** – César Sierra
- **Validation** – Sergio Torres-Cortés; Mauricio Velasquez
- **Visualization** – Sergio Torres-Cortés; Mauricio Velasquez; César Sierra
- **Writing – original draft** – Sergio Torres-Cortés; Mauricio Velasquez
- **Writing – review & editing** – Sergio Torres-Cortés; Mauricio Velasquez

## 7. Acknowledgements

The authors thank to Ministry of Science, Technology, and Innovation and to Universidad Nacional de Colombia – Sede Bogotá.

## 8. References

1. Kim, J., Yun, S., & Ounaies, Z. (2006). Discovery of cellulose as a smart material. *Macromolecules*, 39(12), 4202-4206. <http://doi.org/10.1021/ma060261e>.
2. Habibi, Y., Lucia, L. A., & Rojas, O. J. (2010). Cellulose nanocrystals: chemistry, self-assembly, and applications. *Chemical Reviews*, 110(6), 3479-3500. <http://doi.org/10.1021/cr900339w>. PMID:20201500.
3. Hyde, K., Dong, H., & Hinestroza, J. P. (2007). Effect of surface cationization on the conformal deposition of polyelectrolytes over cotton fibers. *Cellulose (London, England)*, 14(6), 615-623. <http://doi.org/10.1007/s10570-007-9126-z>.
4. Mowafi, S., Rehan, M., Mashaly, H. M., Abou El-Kheir, A., & Emam, H. E. (2017). Influence of silver nanoparticles on the fabrics functions prepared by in-situ technique. *Journal of the Textile Institute*, 108(10), 1828-1839. <http://doi.org/10.1080/00405000.2017.1292649>.
5. Abbas, M., Iftikhar, H., Malik, M. H., & Nazir, A. (2018). Surface coatings of TiO<sub>2</sub> nanoparticles onto the designed fabrics for enhanced self-cleaning properties. *Coatings*, 8(1), 35. <http://doi.org/10.3390/coatings8010035>.
6. Marković, D., Korica, M., Kostić, M., Radovanović, Ž., Šaponjić, Z., Mitrić, M., & Radetić, M. (2018). In situ synthesis of Cu/Cu<sub>2</sub>O nanoparticles on the TEMPO oxidized cotton

- fabrics. *Cellulose (London, England)*, 25(1), 829-841. <http://doi.org/10.1007/s10570-017-1566-5>.
7. Assen, A. H., Yassine, O., Shekhah, O., Eddaoudi, M., & Salama, K. N. (2017). MOFs for the sensitive detection of ammonia: deployment of feu-MOF thin-films as effective chemical capacitive sensors. *ACS Sensors*, 2(9), 1294-1301. <http://doi.org/10.1021/acssensors.7b00304>. PMID:28809112.
  8. Ozer, R. R., & Hinestroza, J. P. (2015). One-step growth of isorecticular luminescent metal-organic frameworks on cotton fibers. *RSC Advances*, 5(20), 15198-15204. <http://doi.org/10.1039/C4RA15161E>.
  9. Smith, M. K., & Mirica, K. A. (2017). Self-Organized Frameworks on Textiles (SOF-T): conductive fabrics for simultaneous sensing, capture, and filtration of gases. *Journal of the American Chemical Society*, 139(46), 16759-16767. <http://doi.org/10.1021/jacs.7b08840>. PMID:29087700.
  10. Wyszogrodzka, G., Marszałek, B., Gil, B., & Dorożyński, P. (2016). Metal-organic frameworks: mechanisms of antibacterial action and potential applications. *Drug Discovery Today*, 21(6), 1009-1018. <http://doi.org/10.1016/j.drudis.2016.04.009>. PMID:27091434.
  11. Horcajada, P., Gref, R., Baati, T., Allan, P. K., Maurin, G., Couvreur, P., Férey, G., Morris, R. E., & Serre, C. (2012). Metal-organic frameworks in biomedicine. *Chemical Reviews*, 112(2), 1232-1268. <http://doi.org/10.1021/cr200256v>. PMID:22168547.
  12. Heinze, T., & Koschella, A. (2005). Carboxymethyl ethers of cellulose and starch - A review. *Macromolecular Symposia*, 223(1), 13-40. <http://doi.org/10.1002/masy.200550502>.
  13. Nooy, A. E. J., Besemer, A. C., & van Bekkum, H. (1995). Highly selective nitroxyl radical-mediated oxidation of primary alcohol groups in water-soluble glucans. *Carbohydrate Research*, 269(1), 89-98. [http://doi.org/10.1016/0008-6215\(94\)00343-E](http://doi.org/10.1016/0008-6215(94)00343-E).
  14. Ovalle-Serrano, S. A., Diaz-Serrano, L. A., Hong, C., Hinestroza, J. P., Blanco-Tirado, C., & Combariza, M. Y. (2020). Synthesis of cellulose nanofiber hydrogels from fique tow and Ag nanoparticles. *Cellulose (London, England)*, 27(17), 9947-9961. <http://doi.org/10.1007/s10570-020-03527-6>.
  15. Saito, T., & Isogai, A. (2004). TEMPO-mediated oxidation of native cellulose. The effect of oxidation conditions on chemical and crystal structures of the water-insoluble fractions. *Biomacromolecules*, 5(5), 1983-1989. <http://doi.org/10.1021/bm0497769>. PMID:15360314.
  16. Biermann, C. J. (1996). *Handbook of Pulping and Papermaking*. London: Academic Press Limited.
  17. Pinto, M. S., Sierra-Avila, C. A., & Hinestroza, J. P. (2012). In situ synthesis of a Cu-BTC metal-organic framework (MOF 199) onto cellulosic fibrous substrates: cotton. *Cellulose (London, England)*, 19(5), 1771-1779. <http://doi.org/10.1007/s10570-012-9752-y>.
  18. Rodríguez, H. S., Hinestroza, J. P., Ochoa-Puentes, C., Sierra, C. A., & Soto, C. Y. (2014). Antibacterial activity against escherichia coli of Cu-BTC (MOF-199) metal-organic framework immobilized onto cellulosic fibers. *Journal of Applied Polymer Science*, 131(19), 40815. <http://doi.org/10.1002/app.40815>.
  19. Emam, H. E., Darwesh, O. M., & Abdelhameed, R. M. (2020). Protective cotton textiles via amalgamation of cross-linked zeolitic imidazole framework. *Industrial & Engineering Chemistry Research*, 59(23), 10931-10944. <http://doi.org/10.1021/acs.iecr.0c01384>.
  20. Zhang, X.-F., Feng, Y., Wang, Z., Jia, M., & Yao, J. (2018). Fabrication of cellulose nanofibrils/UiO-66-NH<sub>2</sub> composite membrane for CO<sub>2</sub>/N<sub>2</sub> separation. *Journal of Membrane Science*, 568, 10-16. <http://doi.org/10.1016/j.memsci.2018.09.055>.
  21. Fu, H., Ou, P., Zhu, J., Song, P., Yang, J., & Wu, Y. (2019). Enhanced protein adsorption in fibrous substrates treated with zeolitic imidazolate framework-8 (ZIF-8) nanoparticles. *ACS Applied Nano Materials*, 2(12), 7626-7636. <http://doi.org/10.1021/acsnam.9b01717>.
  22. Chen, Z., Ma, K., Mahle, J. J., Wang, H., Syed, Z. H., Atilgan, A., Chen, Y., Xin, J. H., Islamoglu, T., Peterson, G. W., & Farha, O. K. (2019). Integration of metal-organic frameworks on protective layers for destruction of nerve agents under relevant conditions. *Journal of the American Chemical Society*, 141(51), 20016-20021. <http://doi.org/10.1021/jacs.9b11172>. PMID:31833359.
  23. Torres-Cortés, S. A., Velasquez, M., Pérez, L. D., & Sierra, C. A. (2022). Ex situ synthesis of MOF@PET/cotton textile fibers as potential antibacterial materials. *Journal of Polymer Research*, 29(10), 427. <http://doi.org/10.1007/s10965-022-03216-x>.
  24. Tranchemontagne, D. J., Hunt, J. R., & Yaghi, O. M. (2008). Room temperature synthesis of metal-organic frameworks: MOF-5, MOF-74, MOF-199, and IRMOF-0. *Tetrahedron*, 64(36), 8553-8557. <http://doi.org/10.1016/j.tet.2008.06.036>.
  25. Kandiah, M., Nilsen, M. H., Usseglio, S., Jakobsen, S., Olsbye, U., Tilset, M., Larabi, C., Quadrelli, E. A., Bonino, F., & Lillerud, K. P. (2010). Synthesis and Stability of Tagged UiO-66 Zr-MOFs. *Chemistry of Materials*, 22(24), 6632-6640. <http://doi.org/10.1021/cm102601v>.
  26. Zhao, H., Kwak, J. H., Conrad Zhang, Z., Brown, H. M., Arey, B. W., & Holladay, J. E. (2007). Studying cellulose fiber structure by SEM, XRD, NMR and acid hydrolysis. *Carbohydrate Polymers*, 68(2), 235-241. <http://doi.org/10.1016/j.carbpol.2006.12.013>.
  27. French, A. D. (2014). Idealized powder diffraction patterns for cellulose polymorphs. *Cellulose (London, England)*, 21(2), 885-896. <http://doi.org/10.1007/s10570-013-0030-4>.
  28. Porras, J. D., Arteta, S. M., & Pérez, L. D. (2020). Development of an adsorbent for Bisphenol A based on a polymer grafted from microcrystalline cellulose. *Water, Air, and Soil Pollution*, 231(10), 499. <http://doi.org/10.1007/s11270-020-04861-y>.
  29. Segal, L., Creely, J. J., Martin, A. E. Jr, & Conrad, C. M. (1959). An empirical method for estimating the degree of crystallinity of native cellulose using the x-ray diffractometer. *Textile Research Journal*, 29(10), 786-794. <http://doi.org/10.1177/004051755902901003>.
  30. Prestipino, C., Regli, L., Vitillo, J. G., Bonino, F., Damin, A., Lamberti, C., Zecchina, A., Solari, P. L., Kongshaug, K. O., & Bordiga, S. (2006). Local structure of framework Cu(II) in HKUST-1 metallorganic framework: spectroscopic characterization upon activation and interaction with adsorbates. *Chemistry of Materials*, 18(5), 1337-1346. <http://doi.org/10.1021/cm052191g>.
  31. Neufeld, M. J., Harding, J. L., & Reynolds, M. M. (2015). Immobilization of Metal-Organic Framework Copper(II) Benzene-1,3,5-tricarboxylate (CuBTC) onto cotton fabric as a nitric oxide release catalyst. *ACS Applied Materials & Interfaces*, 7(48), 26742-26750. <http://doi.org/10.1021/acsmi.5b08773>. PMID:26595600.
  32. Hamisu, A. M., Ariffin, A., & Wibowo, A. C. (2020). Cation exchange in metal-organic frameworks (MOFs): the hard-soft acid-base (HSAB) principle appraisal. *Inorganica Chimica Acta*, 511, 119801. <http://doi.org/10.1016/j.ica.2020.119801>.
  33. DeCoste, J. B., Peterson, G. W., Jasuja, H., Glover, T. G., Huang, Y.-G., & Walton, K. S. (2013). Stability and degradation mechanisms of metal-organic frameworks containing the Zr<sub>6</sub>O<sub>4</sub>(OH)<sub>4</sub> secondary building unit. *Journal of Materials Chemistry. A, Materials for Energy and Sustainability*, 1(18), 5642-5650. <http://doi.org/10.1039/c3ta10662d>.
  34. Abdelhameed, R. M., Rehan, M., & Emam, H. E. (2018). Figuration of Zr-based MOF@cotton fabric composite for potential kidney application. *Carbohydrate Polymers*, 195,

- 460-467. <http://doi.org/10.1016/j.carbpol.2018.04.122>. PMID:29805000.
35. Schelling, M., Kim, M., Ota, E., & Hinestroza, J. (2018). Decoration of cotton fibers with a water-stable metal-organic framework (UiO-66) for the decomposition and enhanced adsorption of micropollutants in water. *Bioengineering (Basel, Switzerland)*, 5(1), 14. <http://doi.org/10.3390/bioengineering5010014>. PMID:29439527.
  36. Wagner, C. D., Riggs, W. M., Davis, L. E., Moulder, J. F., & Muilenberg, G. E. (1979). *Handbook of X-ray Photoelectron Spectroscopy*. USA: Perkin-Elmer Corporation.
  37. Ardila-Suárez, C., Rodríguez-Pereira, J., Baldovino-Medrano, V. G., & Ramírez-Caballero, G. E. (2019). An analysis of the effect of zirconium precursors of MOF-808 on its thermal stability, and structural and surface properties. *CrystEngComm*, 21(9), 1407-1415. <http://doi.org/10.1039/C8CE01722K>.
  38. Tian, S., Yi, Z., Chen, J., & Fu, S. (2023). In situ growth of UiO-66-NH<sub>2</sub> in wood-derived cellulose for iodine adsorption. *Journal of Hazardous Materials*, 443, 130236. <http://doi.org/10.1016/j.jhazmat.2022.130236>.
  39. Ansel, H. C., Norred, W. P., & Roth, I. L. (1969). Antimicrobial activity of dimethyl sulfoxide against *Escherichia coli*, *Pseudomonas aeruginosa*, and *Bacillus megaterium*. *Journal of Pharmaceutical Sciences*, 58(7), 836-839. <http://doi.org/10.1002/jps.2600580708>. PMID:4980332.
  40. Mao, K., Zhu, Y., Rong, J., Qiu, F., Chen, H., Xu, J., Yang, D., Zhang, T., & Zhong, L. (2021). Rugby-ball like Ag modified zirconium porphyrin metal-organic frameworks nanohybrid for antimicrobial activity: synergistic effect for significantly enhancing photoactivation capacity. *Colloids and Surfaces. A, Physicochemical and Engineering Aspects*, 611, 125888. <http://doi.org/10.1016/j.colsurfa.2020.125888>.
  41. Zhao, W., Deng, J., Ren, Y., Xie, L., Li, W., Wang, Q., Li, S., & Liu, S. (2021). Antibacterial application and toxicity of metal-organic frameworks. *Nanotoxicology*, 15(3), 311-330. <http://doi.org/10.1080/17435390.2020.1851420>. PMID:33259255.
  42. Mortada, B., Matar, T. A., Sakaya, A., Atallah, H., Kara Ali, Z., Karam, P., & Hmadeh, M. (2017). Postmetalated zirconium metal organic frameworks as a highly potent bactericide. *Inorganic Chemistry*, 56(8), 4740-4744. <http://doi.org/10.1021/acs.inorgchem.7b00429>. PMID:28338319.

Received: June 27, 2024

Revised: Oct. 05, 2024

Accepted: Nov. 19, 2024

## Supplementary Material

Supplementary material accompanies this paper.

**Scheme S1.** Synthetic conditions and polyhedral representations utilized in the obtention of (a) MOF-99 and (b) MOF UiO-66-NH<sub>2</sub>.

**Scheme S2.** Synthetic pathway for the TEMPO/NaCl/NaClO<sub>2</sub> carboxylation reaction in primary hydroxyl groups on cotton.

**Scheme S3.** Synthetic pathway for the TEMPO/NaCl/NaClO<sub>2</sub> carboxylation reaction in primary hydroxyl groups on cotton.

**Figure S1.** (a) FTIR-ATR spectrum and (b) XRD spectrum of pristine MOF-199 (HKUST-1).

**Figure S2.** (a) FTIR-ATR spectrum and (b) XRD spectrum of pristine MOF UiO-66-NH<sub>2</sub>.

**Figure S3.** EDX spectrum for MOF-199@cotton material.

**Figure S4.** XPS reference spectrum of carboxylated cotton linter. Retrieved with permission of Bastidas Gómez.

**Figure S5.** a) General XPS spectrum of MOF-199@cotton and deconvoluted HR-XPS signals of b) C1s and c) Zn2p<sub>(1/2)</sub> and Zn2p<sub>(3/2)</sub> of MOF-199@cotton.

**Figure S6.** a) General XPS spectrum of MOF UiO-66-NH<sub>2</sub>@cotton and deconvoluted HR-XPS signals of b) C1s and c) N1s of MOF UiO-66-NH<sub>2</sub>@cotton.

**Figure S7.** EDX spectrum for MOF UiO-66-NH<sub>2</sub>@cotton material.

**Figure S8.** Petri dishes with solid agar cultures and for a) *E. coli* and b) *S. aureus* after 48 h. For both of them, numbers corresponds to: 1: Cu-alg (Cotton composite anchored to MOF 2: Cu-PET (PET-cotton composite anchored to MOF-199), 3: Zr-alg (Cotton composite anchored to MOF UiO-66-NH<sub>2</sub>), 4: Zr-PET (PET-cotton composite anchored to MOF UiO-66-NH<sub>2</sub>), 5: Blanco PET (PET-cotton composite blank), 6: Algodon ⊕ (Positive control for cotton consisting of cotton fiber rinsed in DMSO), 7: PET ⊕ (Positive control for PET-cotton rinsed in DMSO), 8: Blanco alg. (cotton composite blank).

**Figure S9.** Inhibition curves in liquid cultures of cotton blank (red), MOF-199@cotton (purple), and MOF UiO-66-NH<sub>2</sub>@cotton (orange) for (a) *E. coli* and (b) *S. Aureus*.

**Figure S10.** Inhibition activity expressed as the number of bacteria after 48 h of experiment (green columns) and inhibition percentage (blue columns) for cotton blank, MOF-199@cotton and MOF UiO-66-NH<sub>2</sub>@cotton for a) *E. coli* and b) *S. aureus*.

This material is available as part of the online article from <https://doi.org/10.1590/0104-1428.20240068>